High sensitivity electron diffraction analysis

A study of divalent cation binding to purple membrane

Alok K. Mitra and Robert M. Stroud
Department of Biochemistry and Biophysics, University of California San Francisco, San Francisco, California 94143-0448

ABSTRACT A sensitive high-resolution electron diffraction assay for change in structure is described and harnessed to analyze the binding of divalent cations to the purple membrane (PM) of *Halobacterium halobium*. Low-dose electron diffraction patterns are subject to a matched filter algorithm (Spencer, S. A., and A. A. Kossiakoff. 1980. *J. Appl. Crystallogr.* 13:563–571). to extract accurate values of reflection intensities. This, coupled with a scheme to account for twinning and specimen tilt in the microscope, yields results that are sensitive enough to rapidly quantitate any structure change in PM brought about by site-directed mutagenesis to the level of less than two carbon atoms.

Removal of tightly bound divalent cations (mainly Ca^{2+} and Mg^{2+}) from PM causes a color change to blue and is accompanied by a severely altered photocycle of the protein bacteriorhodopsin (bR), a light-driven proton pump. We characterize the structural changes that occur upon association of 3:1 divalent cation to PM, versus membranes rendered purple by addition of excess Na^+. High resolution, low dose electron diffraction data obtained from glucose-embedded samples of Pb^{2+} and Na^+ reconstituted PM preparations at room temperature identify several sites with total occupancy of 2.01 ± 0.05 Pb^{2+} equivalents. The color transition as a function of ion concentration for Ca^{2+} or Mg^{2+} and Pb^{2+} are strictly comparable. A (Pb^{2+} – Na^+) PM Fourier difference map in projection was synthesized at 5 Å using the averaged data from several nominally untilted patches corrected for twinning and specimen tilt. We find six major sites located on helices 7, 5, 4, 3, 2 (nomenclature of Engelman et al. 1980. *Proc. Natl. Acad. Sci. USA.* 77:2023–2027) in close association with bR. These partially occupied sites (0.55–0.24 Pb^{2+} equivalents) represent preferential sites of binding for divalent cations and complements our earlier result by x-ray diffraction (Katre et al. 1986. *Biophys. J.* 50:277–284).

INTRODUCTION

Bacteriorhodopsin (bR), a transmembrane protein, is found in a highly ordered, two-dimensional hexagonal P3 lattice as purple patches (the so-called purple membrane [PM]) in the cytoplasmic membrane of halophilic bacterium *Halobacterium halobium* (Stoeckenius and Bogomolni, 1982). bR contains a single retinylidene chromophore bound via a protonated Schiff base to the ϵ-NH_2 group of Lys216 (Bayley et al., 1981; Katre et al., 1981) and absorbs maximally at 568 nm in the light-adapted form of native bR. Upon the absorption of a photon, bR undergoes a photocycle during which all-*trans* to 13-*cis* isomerization of the chromophore plus deprotonation of the Schiff base takes place and protons are pumped vectorially to the extracellular region, establishing an electrochemical gradient which drives some metabolic processes, e.g., ATP synthesis (Bogomolni et al., 1976).

Well-washed PM binds primarily divalent cations, namely, ~3–4 mol of Mg^{2+} and ~1 mol of Ca^{2+} per mol of bR and small amounts of manganese, copper, and zinc (Chang et al., 1985). Deionization of PM turns the membrane blue with λ_{max} shifting to 605 nm (Kimura et al., 1984), and this color transition is associated with a severely altered photocycle (Kobayashi et al., 1983). The blue membrane photocycle lacks a deprotonated blue-shifted photo-intermediate analogous to M_{412}, and it has been suggested (Mowery et al., 1979) that it does not pump protons. PM can be regenerated by the addition of stoichiometric amounts of divalent cations (2–3 times) or monovalent cations (200 times) to the deionized PM (Kimura et al., 1984; Chang et al., 1985, 1986). Recent studies have shown, for instance, through absorption spectroscopy (Kimura et al., 1984; Chang et al., 1985; Ariki and Lanyi, 1986) and electron spin resonance spectroscopy (Duñach et al., 1987) that there are multiple tight binding sites for divalent cations on the PM. The involvement of metal ions in the deprotonation of the Schiff base and a tyrosine residue during the formation of M_{412} have been described (Corcoran et al., 1987; Dupuis et al., 1985). These observations have suggested a possible role for the divalent cations in the functioning of bR (Dupuis et al., 1985; Chronister and El-Sayed, 1987), either by direct involvement in the proton-pumping mechanism or in maintaining structural integrity. However, recent studies (Szundi and Stoeckenius, 1987, 1988)

suggest that the blue to purple transition is mediated only by protonation changes at the membrane surface and apparently argue against any direct role for the divalent cations with regard to the stabilization of bR and/or proton pumping.

In this study by electron diffraction on glucose embedded single PM sheets, we investigated whether or not there are discrete divalent-cation binding sites on PM, and if so define their location in projection. High-resolution electron-diffraction data from purple membrane sheets reconstituted with Pb^{2+} or with Na^+, whereby possible effects on the protein conformation through deionization were minimized, were compared by the calculation of a difference density map between the former and the latter to locate divalent-cation binding sites. The color transition as a function of the ion concentration for Ca^{2+} or Mg^{2+} and Pb^{2+} are strictly comparable. Also Pb^{2+} and Na^+ were chosen so as to maximize the contribution of the difference in electron scattering potential in the two cases and hence the signal in the difference map. By establishing the validity of a $Pb^{2+} - Na^+$ peak (Katre et al., 1984) in the difference Fourier map, we describe the sites of divalent cation binding on PM. The six major sites, all located on the protein, are partially occupied (0.55–0.24 Pb^{2+} equivalents) and establish preferential binding sites for divalent cation. This conclusion complements results from our earlier investigation based on x-ray diffraction analyses (Katre et al., 1986).

MATERIALS AND METHODS

Materials

Purple membranes isolated from strain ET1001 of *H. halobium* (Oesterhelt and Stoeckenius, 1974) were provided by Prof. W. Stoeckenius (Cardiovascular Research Institute, University of California, San Francisco, CA). The concentration of bR in PM was assayed by absorbance at 568 nm using a value of 63,000 $cm^{-1}M^{-1}$ for the extinction coefficient of light-adapted form of bR. The concentration of bR in blue membrane (BM: deionized PM) was measured using ϵ_{605} = 60,000 $cm^{-1}M^{-1}$ (Kimura et al., 1984). Optical densities were measured on a spectrophotometer (Beckman Instruments, Inc., Fullerton, CA) equipped with a digital detection system (Gilford Instruments Laboratories, Inc., Oberlin, OH). All centrifugations were carried out in a Sorvall SS-34 rotor (DuPont Co., Wilmington, DE) at 4°C. Cation-exchange resin in hydrogen form was cellex-P (Bio-Rad Laboratories, Richmond, CA). All blue membrane preparations were kept in clean plastic tubes (Applied Scientific, San Francisco, CA) as suspension in nano-pure water (18 MΩ/cm restivity, pH 5.9) (Sybron/Barnstead, Boston, MA) at 4°C and handled with plastic pipettes (Bio-Rad Laboratories). Any contact with glass was scrupulously avoided. Triton X-100 (Rohm and Haas Co., Philadelphia, PA), D-glucose, and the salts NaCl, $PbCl_2$, NaH_2PO_4, Na_2HPO_4, $NaCH_3COO$, and NaN_3 were reagent grade.

Specimen preparation

To improve signal-to-noise ratio in electron diffraction patterns, we used large reconstituted PM sheets (5 μm average diameter, ≈10^6 molecules of bR per diffraction pattern) prepared by Triton X-100 solubilization followed by detergent removal (Cherry et al., 1978). Blue membranes generated from such PM sheets by the passage through a cation exchange resin (Kimura et al., 1984; Katre et al., 1986) were converted to purple membrane by adding either Pb^{2+} or Na^+.

Glucose embedded Pb^{2+} or Na^+ reconstituted PM samples were prepared for electron diffraction as follows. For preparing Pb^{2+} labeled PM samples, an aliquot of BM (60–80 μM protein concentration) was incubated overnight with 3:1 molar ratio of $PbCl_2$ to protein. This Pb^{2+}-labeled membrane was later resuspended at the same protein concentration in 1 mM Na phosphate buffer, pH 7.0, containing 0.7% glucose and 0.05% sodium azide. Na^+-reconstituted PM samples were prepared by resuspending BM (60–80 μM protein concentration) in 10 mM sodium (Na^+/bR ≈ 150:1) phosphate buffer pH 7.0 containing 0.7% glucose and 0.05% sodium azide. Hereafter, Na^+- and Pb^{2+}-reconstituted samples are referred to as Na^+ PM and Pb^{2+} PM, respectively.

Electron microscopy

Typically 6 μl of glucose-embedded reconstituted PM sample was applied to a 300-mesh copper grid that was covered by a thin hydrophobic carbon film floated off a freshly-cleaved mica sheet. The carbon-coated grid was washed several times with nanopure water before sample application. The sample was allowed to stand for ~5 min and then excess liquid was removed by touching the edge of the grid with the tip of a filter paper, and the grid air dried. Electron diffraction was carried out at 100 kV in an EM400 electron microscope (Phillips Electronic Instruments, Eindhoven, Netherlands). Electron dose (e/Å²/min) on the specimen was determined by measured current registered on an electrometer (model 610B; Keithley Instruments, Inc., Cleveland, OH) connected to the focusing screen. A current versus dose calibration determined from the knowledge of the speed of the recording film was used for this purpose.

A nominal dose rate of 2.0–2.5 e/Å²/min was set up by using a spot size of 0.5 μm (highly excited first condenser lens), 12-μm-diam condenser aperture, and an illuminated area of ~8 μm on the specimen by overfocusing the second condenser lens. With the emission current turned down to the lowest setting, the grid was scanned in an out-of-focus diffraction mode which resulted in a high contrast image. When a suitable membrane sheet was found, the diffraction beam was rapidly focused, the beam shuttered, and the emission current restored to normal. This resulted in no more than ~0.03 e/Å² of total dose on the crystal before taking the exposure. Next the shutter was opened and an exposure taken typically for 10 s which resulted in a total dose of ~0.3–0.4 e/Å². At the end of each session of recording diffraction patterns, calibration films with known electron exposures were obtained. Diffraction patterns and calibration films were recorded on Kodak 4489 film (Eastman Kodak Co., Rochester, NY), which was developed for 4 min according to manufacturer's specification in fresh Kodak D19 developer diluted 1:2 with deionized water at 20°C.

Data acquisition

Electron diffraction patterns that showed reflections to high resolution, typically to ~3.5 Å, were digitized on a PDS 1010M flatbed microdensitometer (Perkin-Elmer Corp., Norwalk, CT) using an aperture and step size of 10 μm. To reduce the area of scanning and yet have enough data points for reliable estimation of background, strips 49 pixels wide and centered on lattice rows parallel to one of the unit cell axes were scanned for reflection intensities from infinity to 3.5 Å resolution and digitized. From scanning the calibration films it was found that for the "slow" Kodak 4489 films used in this study up to an optical density (OD) of 2.8

corresponding to that for the strongest reflections, the OD values were linearly related to electron exposure with a correlation coefficient >0.99. Hence no conversion factor for determining electron exposure was used and this was absorbed in the final scaling of the diffraction patterns. Smoothing of the data, accurate location of the diffraction spot centers, and calculation of the background and the background-corrected intensities were carried out using a "matched filter" algorithm (Spencer and Kossiakoff, 1980) as described in Katre et al. (1984).

Correction for twinning, tilt, and scaling

The large reconstituted PM sheets used for data collection are in general twinned, being composed of domains of bR molecules in opposite orientations and organized according to the space group P3. A scheme for the analysis of the twins, detwinning, and removal of the effects of the specimen tilt in terms of departure from exact normal to the electron beam (even a small amount of which introduces systematic errors in intensities, especially at high resolution) was developed as described in the Appendix. Nominally untilted patterns were selected visually by comparing the intensities of the symmetry mates of tilt sensitive reflections 5,0 and 7,0 whose intensities are twin independent, and 1,4 and 4,2. Systematic errors arising from specimen tilt were corrected for the 26-7 Å data by using the variation of structure factor against z^*, the distance along the reciprocal lattice line. For reflections from 7 to 5 Å resolution a linear fit of the intensities of symmetry-related reflections to z^* was applied to determine the tilt contribution. The symmetry, Friedel, and triplet residuals R_S, R_F, and R_T, respectively, for a diffraction pattern were calculated as,

$$R_S = \sum_{hk}\sum_{i=1}^{n}\left| |F_i| - \langle |F_i| \rangle \right| \Big/ \sum_{hk}\sum_{i=1}^{n} |F_i| \qquad (1)$$

$$R_F = \sum_{hk}\sum_{i=1}^{n}\left| |F_i| - |F_{\bar{i}}| \right| \Big/ \sum_{hk}\sum_{i=1}^{n} (|F_i| + |F_{\bar{i}}|) \qquad (2)$$

$$R_T = \sum_{hk}\sum_{i=1}^{n}\left| |F_{ii}| - \langle |F_{ii}| \rangle \right| \Big/ \sum_{hk}\sum_{i=1}^{n} |F_{ii}|, \qquad (3)$$

where F's are the extracted detwinned–detilted amplitudes, $\langle |F_i| \rangle$ is the sixfold symmetry-averaged value, $\langle |F_{ii}| \rangle$ is the triplet averaged value, $\bar{i}$ is the Friedel mate of reflection i and $|F_{ii}| = (|F_i| + |F_{\bar{i}}|)/2.0$.

The extracted diffraction amplitudes after correcting for twinning and tilt were sixfold symmetry averaged and then weighted according to their variance between patterns. The Na^+ PM patterns were scaled and averaged together to yield a set of consensus Na^+ PM amplitudes $F_N(hk)$. The extracted symmetry averaged amplitudes from each Pb^{2+} PM pattern were individually scaled to $F_N(hk)$ set and subsequently averaged between patterns after weighting according to the variance, to yield a set of consensus Pb^{2+} PM amplitudes $F_D(hk)$. The scaling between two sets of amplitudes F_1 and F_2 was performed by least-squares minimizing

$$Q = \sum_{hk} \langle F_1 \rangle_s - K \exp(-Bs^2) \langle F_2 \rangle_s, \qquad (4)$$

where s is the reciprocal lattice vector and sum is over all overlapping reflections. The scaling residual after minimization was given by

$$R = Q / \sum_{hk} \langle F_1 \rangle_s. \qquad (5)$$

Fourier analysis and error estimation in the maps

Difference Fourier maps were generated from the Fourier synthesis of the terms ΔF, where

$$\Delta F = (|F_1(hk)| - |F_2(hk)|) \cdot m_{hk} \cdot \exp(i\phi_{hk}). \qquad (6)$$

Here F_1 corresponds to $F_D(hk)$ or a subset of Pb^{2+} PM patterns and F_2 corresponds to $F_N(hk)$ or a subset of Na^+ PM patterns, m_{hk} is the figure of merit, and ϕ_{hk} the projection phase as determined by Hayward and Stroud (1981).

The interpretation of a peak or a set of peaks in the difference Fourier map as potential candidates for Pb^{2+} sites was tested by refining the positions and occupancies of the selected sites by the least squares minimization of

$$E = \sum_{hk} (|F_D| - |F_N + f_{pb}|)^2, \qquad (7)$$

where f_{pb} is the calculated structure factor contribution from Pb^{2+} and the sum is over all independent reflections (Dickerson et al., 1968). Double difference Fourier maps synthesized with terms $\Delta\Delta F_{pb}$, where

$$\Delta\Delta F_{pb} = (|F_D| - |F_N + f_{pb}|) \cdot m_{hk} \cdot \exp(i\phi_{hk}), \qquad (8)$$

then show possible errors and/or extra features (with a better signal-to-noise ratio than difference maps) still unaccounted for in the model for the cation sites.

The mean squared error $\langle \Delta\Delta\rho^2 \rangle$ in the difference map was calculated according to the expression (Blundell and Johnson, 1976)

$$\langle \Delta\Delta\rho^2 \rangle = (1/V^2) \sum_{hk} 0.5 \cdot [\Delta F(hk)]^2 + \sigma_N(hk)^2 + \sigma_D(hk)^2, \qquad (9)$$

where σ_N and σ_D are the standard deviations in F_N and F_D (Table 2), ΔF is the difference amplitude, and the sum is over all reflections used in the synthesis of the map. The standard deviation in the expected noise level is $\Omega = (\langle \Delta\Delta\rho^2 \rangle)^{1/2}$.

All data between 26 and 5 Å were used in scaling, averaging, Fourier synthesis, and in refinement of sites.

An absolute scale factor for the native amplitudes was calculated by assuming that the protein occupies 68% of the unit cell and that the average scattering density in the lipid region is 77% of that of the protein (Engelman et al., 1980). Electron scattering factors were from International Tables for Crystallography, vol. 4.

RESULTS

Statistics of extracted amplitudes

The expected average change in the electron structure factors for the addition of 2 Pb^{2+} is 10% and is 12% for 3 Pb^{2+} on the assumption that the protein is a random arrangement of ordered atoms as are the lipid molecules. Neither of these two assumptions is strictly correct because of coherently or repetitively disposed atomic positions in helices and because results from structural analysis of bR (Hayward and Stroud, 1981; Baldwin et al., 1988) and from partially delipidated bR (Glaeser et al., 1985; Tsygannik and Baldwin, 1987) indicate that at

least some of the lipid molecules are ordered. This means that the average change in F's are expected to be even lower than the values indicated above, and so it was critically important to minimize all sources of error.

Since Friedel-related reflections are unaffected by twinning and specimen tilt, only those nominally untilted diffraction patterns that had the least noise as assayed by the low values of the residual R_F were considered for averaging. 4 Na^+ PM patterns and 6 Pb^{2+} PM patterns were chosen. The statistics for these patterns after detwinning and detilting are given in Table 1. All except two of the diffraction patterns were essentially untwinned: the amount of twinning in these two were 28.07 (±0.40)% and 1.07(±0.40)%. The Friedel residuals (5% on an average) here are about one half of that observed earlier for native or mercurilated phenyl-glyoxal labeled PM (Katre et al., 1984) and the reduction in noise is essentially due to better signal-to-noise ratio in the diffraction patterns from ~25 times larger reconstituted sheets used in this work. The systematic errors in each pattern resulting from errors in evaluating the twinning and tilt parameters and from their contribution to the calculation of corrected amplitudes are represented in the "triplet" residuals R_T (Table 1) calculated for threefold symmetric reflections where each reflection is averaged with its Friedel mate. Table 2 lists the averaged extracted amplitudes F_N and F_D and their standard deviations (Bevington, 1969) calculated from a total of 24 (4 Na^+ PM

TABLE 1 Statistics* for diffraction patterns from reconstituted PM used for calculating Fourier difference maps

	Na^+ PM	Pb^{2+} PM
No. of patterns averaged	4	6
R_F‡ (26–5 Å)	4.0–5.5 (4.6)§	4.1–6.3 (5.0)
(26–7 Å)	2.6–3.4 (3.0)	2.7–5.0 (3.5)
(7–5 Å)	6.3–9.9 (7.6)	6.6–9.5 (6.7)
R_T‡ (26–5 Å)	2.9–3.9 (3.4)	3.5–6.5 (4.7)
(26–7 Å)	1.9–2.5 (2.3)	2.6–5.6 (3.5)
(7–5 Å)	4.5–6.5 (5.2)	5.2–7.6 (6.4)
Tilt‖	0.3–0.9	0.1–0.5
R¶	4.6–6.2 (5.3)	4.0–7.4 (5.4)

*Based on extracted detwinned-detilted amplitudes.
‡Agreement index (see Materials and Methods for definition) in percentage for a diffraction pattern.
§Entries in parentheses are averaged values.
‖Estimated specimen tilt in degree with average values of 0.6 ± 0.1 degree for Na^+ PM patterns and 0.4 ± 0.2 degree for the Pb^{2+} PM patterns.
¶Calculated scaling residual between patterns after sixfold averaging of the symmetry-related relfections (see Materials and Methods for definition).

TABLE 2 Averaged structure factors F * and their experimentally determined deviations σ‡ for Na^+ reconstituted (F_N) and Pb^{2+} reconstituted (F_D) purple membrane to 5 Å resolution

H	K	F_N	σ_N	F_D	σ_D
1	2	9.36	0.09	9.76	0.09
1	3	4.37	0.16	4.85	0.09
1	4	13.50	0.16	13.72	0.07
1	5	16.38	0.10	16.12	0.08
1	6	3.53	0.08	3.38	0.06
1	7	13.24	0.12	13.09	0.08
1	8	4.61	0.17	4.33	0.10
1	9	4.49	0.15	3.38	0.19
1	10	3.81	0.12	4.31	0.08
2	1	5.29	0.22	5.61	0.24
2	2	13.09	0.09	13.27	0.15
2	3	8.19	0.08	8.88	0.13
2	4	22.59	0.16	22.55	0.15
2	5	6.47	0.17	6.78	0.08
2	6	8.28	0.04	8.10	0.07
2	7	9.04	0.17	9.26	0.04
2	8	8.77	0.25	9.23	0.06
2	9	8.28	0.37	8.50	0.06
3	0	4.71	0.13	4.76	0.11
3	1	15.30	0.15	15.22	0.11
3	2	12.17	0.05	13.13	0.16
3	3	2.77	0.18	3.42	0.10
3	4	16.97	0.06	16.49	0.06
3	5	16.28	0.13	16.16	0.08
3	6	2.67	0.13	2.98	0.09
3	7	6.96	0.12	6.83	0.06
3	8	5.54	0.14	5.03	0.19
4	0	12.43	0.09	12.96	0.12
4	1	15.72	0.12	15.49	0.05
4	2	8.01	0.19	8.02	0.11
4	3	27.43	0.21	26.54	0.29
4	4	5.91	0.12	6.34	0.16
4	5	6.01	0.10	5.69	0.12
4	6	3.17	0.23	3.31	0.05
4	7	4.52	0.06	4.43	0.07
4	8	3.96	0.21	4.34	0.10
5	0	19.09	0.06	18.60	0.04
5	1	4.15	0.19	4.07	0.07
5	2	18.15	0.22	17.95	0.07
5	3	5.86	0.07	6.66	0.12
5	4	3.26	0.08	3.01	0.11
5	5	3.90	0.14	3.92	0.03
5	6	2.64	0.13	3.15	0.14
5	7	5.52	0.06	5.51	0.74
6	0	11.36	0.03	11.30	0.07
6	1	13.71	0.11	14.13	0.12
6	2	5.81	0.07	5.71	0.11
6	3	2.07	0.01	2.35	0.07
6	4	5.69	0.07	5.78	0.05
6	5	3.26	0.17	2.42	0.34
6	6	2.05	0.05	1.80	0.23
7	0	9.77	0.06	9.78	0.03
7	1	9.35	0.04	9.19	0.10
7	2	2.69	0.21	2.70	0.12
7	3	4.99	0.07	4.96	0.09
7	4	2.02	0.15	2.53	0.24
7	5	2.47	0.03	2.47	1.14
8	0	2.99	0.25	3.35	0.10

TABLE 2 (continued)

8	1	2.12	0.05	2.20	0.08
8	2	5.96	0.09	6.34	0.07
8	3	5.54	0.14	6.09	0.07
8	4	3.14	0.14	3.27	0.03
9	0	3.54	0.09	4.12	0.18
9	1	8.29	0.10	8.61	0.05
9	2	4.96	0.18	5.00	0.08
10	0	2.95	0.11	3.33	0.15
10	1	3.44	0.10	2.92	0.16

*Each F_N and F_D are averages of 24 and 36 separate observations, respectively, for the same reflection.

$$F = \sum_{j=1}^{M} (F_j/\sigma_j^2) / \sum_{j=1}^{M} (1/\sigma_j^2),$$

where σ_j is the standard deviation in the extracted sixfold averaged structure factor F_j for the jth pattern and M is the number of patterns averaged.

$$^{\ddagger}\sigma = \left[\sum_{j=1}^{M} (1/\sigma_j^2)(F_j - F)^2/M \sum_{j=1}^{M} (1/\sigma_j^2)\right]^{1/2},$$

where F is F_N or F_D.

patterns) and 36 (6 Pb^{2+} PM patterns) observations for the 67 independent reflections (26–5 Å).

Fourier difference maps and error analyses

The consensus difference map calculated using the sets of amplitudes F_N and F_D is shown in Fig. 1 *a* where the six major refinable sites for cation binding are marked. Fig. 1 *b* shows that all these six sites are within the protein boundary.

To assess the effects of random errors in the amplitudes in our (Pb^{2+} – Na^+) consensus difference map, we carried out difference Fourier analyses on independent subsets of data. We first looked at the contribution of noise in the Na^+ PM and Pb^{2+} PM data sets. For this purpose we synthesized difference maps between independent subsets of two merged Na^+ PM and also between independent subsets of two merged Pb^{2+} PM data. A typical set of such "noise" maps are shown in Fig. 2. The "noise" map synthesized from the Pb^{2+} PM data shows no distinct features while the "noise" map synthesized from Na^+ PM data also is essentially featureless except for two peaks that are closest to, but distinct from, the peak at helix 7 in the consensus difference map in Fig. 1 *a*. Next we studied Pb^{2+} – Na^+ subset difference maps. These are difference maps synthesized from independent subsets of data from two merged Pb^{2+} PM and two merged Na^+ PM data. These independent sets of difference amplitudes showed a high degree of similarity with an average sample correlation coefficient (Hoel, 1984) of 0.64. In

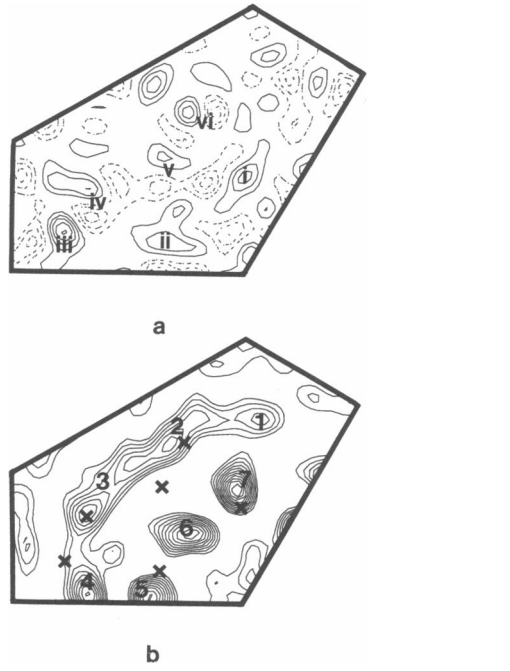

FIGURE 1 (*a*) Consensus projected Fourier difference map calculated at 5 Å resolution with the six major refinable divalent cation sites marked. The contour interval is one standard deviation of the expected noise level (Ω, see Materials and Methods). Solid lines represent positive and dashed lines represent negative contour levels (*b*). The refined cation-site locations indicated as crosses relative to the projected electron scattering density of PM at 5 Å resolution.

Fig. 3 a collection of such subset difference maps contoured at the same density interval as the previous maps are shown. These maps show in general a mutual similarity in the pattern of all significant peaks in strength and their positions, comparable to those seen in Fig. 1 *a*, even though because of the averaging of fewer data sets these maps are, as expected, noisier than the consensus difference map. Taken together, the maps in Figs. 2 and 3 establish clearly that the peaks in the consensus map (Fig. 1 *a*) are not due to random errors in the amplitudes.

Refinement of the peaks

In order to assess whether a statistically significant peak in Fig. 1 *a* is a positive peak due to Pb^{2+} and not due to some structural change in the protein, least-squares refinement of the positions and occupancies of the sites was followed by the calculation of double-difference Fourier maps (Katre et al., 1984, 1986). Ideally, any net negative peaks remaining would then indicate conformational change. All statistically significant peaks (peak height ≥ 2 Ω) were analyzed. First, individual peaks were separately refined and, in each case, in the accompanying

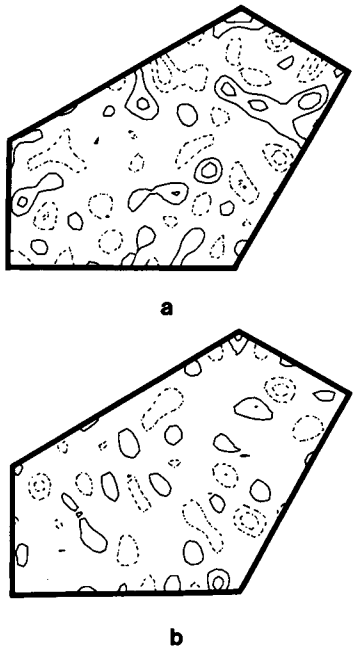

FIGURE 2 Assay of noise in Na^+ PM (*a*) and Pb^{2+} PM (*b*) data. Difference maps between two independent subsets each derived (*a*) from two merged Na^+ PM data sets and (*b*) from two merged Pb^{2+} PM data sets. The contour interval is the same as in Fig 1 *a*.

double-difference map peaks that appeared back at or above 2 Ω were noted. Different combinations of peaks that survived this initial refinement were then simultaneously refined, followed again by the calculation of the double-difference maps. Several sets of such calculations revealed that only the peaks marked in Fig. 1 *a* refined satisfactorily and also were in mutual agreement in the double-difference maps. In Fig. 1 *b* the final refined positions of the cation-binding sites are indicated relative to the projected electron scattering density of PM. The final double difference map (Fig. 4) after the refinement of the peaks marked in Fig. 1 *a* is essentially featureless. This shows that the model of Pb^{2+} sites completely accounts for the observed difference in *F*'s between the consensus Pb^{2+} PM and consensus Na^+ PM data sets.

Based on the calculated absolute scale factor, the occupancies in terms of Pb^{2+} equivalents at the major refinable sites are shown in Table 3. Each site is partially occupied ranging in occupancy of 0.24–0.55 and the total calculated Pb^{2+} occupancy is 2.01 ± 0.05 in comparison to the maximum possible value of 3 for our 3:1 Pb^{2+} to bR reconstitution. This calculated occupancy agrees with the value for the average observed fractional change $\langle|\Delta F|\rangle / \langle|F_N|\rangle$, which was 3.0% in the resolution range 26–7 Å and 6.9% in the resolution range 7–5 Å.

To further test the sensitivity achieved in our consensus difference Fourier map (Fig. 1 *a*) we performed the

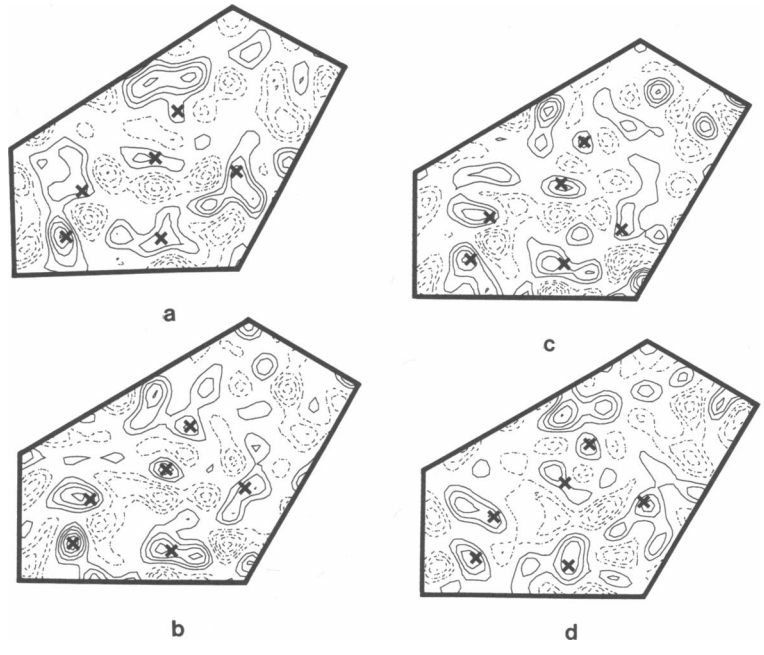

FIGURE 3 Difference maps calculated between different independent subsets of merged Pb^{2+} PM and merged Na^+ PM data. The difference amplitudes used to generate the pairs of maps *a*, *b* and *c*, *d* arise from conjugation of entirely independent Na^+ PM and Pb^{2+} PM data sets. The contour interval is the same as in Fig. 1 *a*.

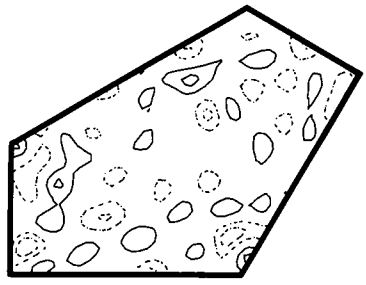

FIGURE 4 Final double difference map after the refinement of the six located divalent cation sites. The contour interval is the same as in Fig. 1 *a*.

following analysis on peak 4 which yields the lowest refined occupancy of 0.24 Pb^{2+}. In Fig. 5 *a* the idealized signal due to 0.24 Pb^{2+} located at the refined site is shown. Assuming that the random noise in the difference amplitudes follow a normal distribution, we calculated a noise-corrupted set ΔF_{Pb}^{noise} by adding (or subtracting) randomly to the idealized set ΔF_{Pb} the experimentally observed noise in $|\Delta F|$ weighted by a Gaussian based on spline-fitted values of averaged observed noise versus resolution (Fig. 6) and their standard deviations. In Fig. 5 *b* the map synthesized based on these calculated "noisy" difference amplitudes is shown in which the most intense peak is still seen at the same location but the peak height is reduced by about 22% compared with that for the idealized signal in Fig. 5 *a*. Thus the signal due to 0.24 Pb^{2+} can be clearly distinguished from random noise in our consensus difference map. To address the same issue the maps in Fig. 2, *a* and *b*, which describe noise in the Na^+ and Pb^{2+} PM data sets, were further analyzed. At each of the Pb^{2+} sites cited in Fig. 1 *a*, the singly-refined occupancies at the corresponding locations in both the noise maps were calculated. The largest values for these occupancies were 0.10 and 0.12 Pb^{2+} equivalents for the

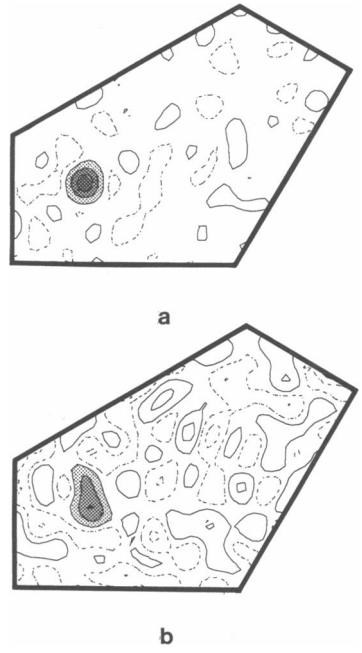

FIGURE 5 (*a*) An ideal difference map, synthesized by adding contributions for 0.24 Pb^{2+}, the lowest refined occupancy deduced from the consensus difference map (Fig. 1 *a*) to the observed structure factors for Na^+ PM and then generating difference terms ΔF and (*b*) corresponding expected noise-corrupted map based on the experimentally determined errors in the amplitudes of both Na^+ PM and Pb^{2+} PM. The ideal peak in *a* and the noise-corrupted peak in *b* are shaded. The contour interval is 0.88 Ω.

maps in Fig. 2, *a* and *b*, respectively. By either estimate even the largest noise peak in the "noise" maps translate to less than half the lowest observed occupancy level of 0.24 Pb^{2+} equivalents in the consensus difference map (Fig. 1 *a*).

TABLE 3 Occupancy of the divalent cation binding sites in purple membrane

Site	Location*	Occupancy in Pb^{2+} equivalents‡
(i)	Helix 7	0.27
(ii)	Helix 5	0.41
(iii)	Helix 4	0.55
(iv)	Helix 3	0.24
(v)	Helix 2 and 3	0.27
(vi)	Helix 2	0.27
	Total	2.01

*Closest helix location in the projected structure.
‡The estimated average error in occupancy at a given site is 0.01 Pb^{2+} equivalent calculated from the least-squares refinement analysis.

Scattering and errors in the consensus data sets

In Fig. 6, the level of estimated errors in $|\Delta F|$, extracted after detwinning and correcting for tilt, sixfold observations of each reflection from 4 Na^+ PM and 6 Pb^{2+} PM patterns, observed and calculated values of $|\Delta F|$ after refinement of positions and occupancies of the cation sites, and the lack of closure errors are illustrated. Relative to $\langle|F_N|\rangle$ the average estimated error in $|\Delta F|$ is 2.4% and the lack of closure error $|\Delta\Delta F|$ is 2.8% and thus are comparable throughout the resolution range. The observed average fractional change $\langle|\Delta F|\rangle / \langle|F_N|\rangle$ ranged from 3.0% at low resolution (26–7 Å) to 6.9% at higher resolution (7–5 Å).

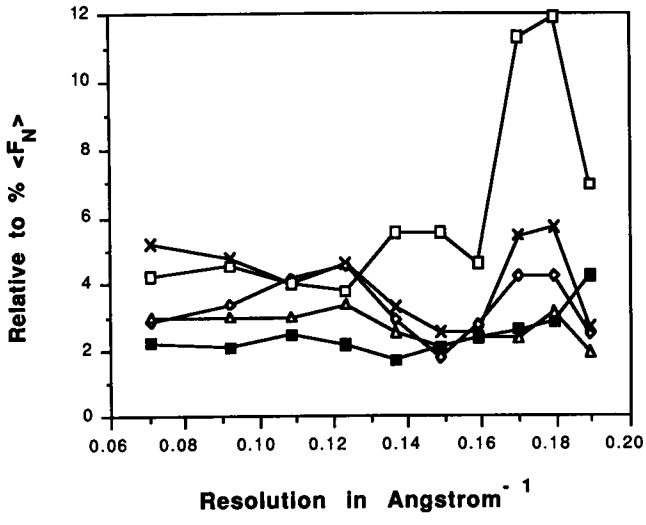

FIGURE 6 Scattering and errors for the Pb^{2+} reconstituted PM versus resolution. x, mean observed difference $\langle|\Delta F|\rangle$ between Pb^{2+} PM and Na^+ PM structure factors; ◇, calculated value of $\langle|\Delta F|\rangle$ computed from $\|F_N + f_{pb}| - |F_N\|$ after refinement; Δ, lack of closure errors $\langle|\Delta\Delta F|\rangle$ computed from $\|F_D| - |F_N + f_{pb}\|$ after refinement; and ■, mean error in $|\Delta F|$ calculated from 24 and 36 observations of each reflection from the sets of 4 Na^+ PM and 6 Pb^{2+} PM data sets, respectively, given as square root $(\sigma_N^2 + \sigma_D^2)$, where σ's are listed in Table 2. Each point on the graph is for a bin of 12 reflections centered at that resolution.

DISCUSSION

We have located Pb^{2+} binding sites on PM by low-dose electron diffraction on glucose-sustained single purple membrane sheets. There are six major sites located on helices 7, 5, 4, 3, and 2 (nomenclature of Engelman et al., 1980) all of which are partially occupied ranging in occupancy from 0.55 to 0.24 of Pb^{2+} equivalents with the total occupancy of 2.01 ± 0.05 compared with the total titrated amount of 3 Pb^{2+}/bR in the samples used for electron diffraction. There are also peaks in the lipid region that do not mutually refine satisfactorily with the peaks at the major sites. These peaks at the lipid region could arise due to phase errors inherent in the difference Fourier synthesis; however, it cannot be ruled out that these may also represent additional binding sites. From the present work the three-dimensional location of the sites cannot be deduced; however, recent results from anomalous small angle x-ray scattering (Wakatsuki, S., S. Doniach, and K.O. Hodgson, manuscript in preparation) on Tb^{3+}-titrated bR clearly show that cations bind exclusively on the membrane surface.

The use of large reconstituted sheets (~5 μm diam) which improved the signal-to-noise ratio in our diffraction patterns, the use of a matched-filter algorithm (Spencer and Kossiakoff, 1980) to evaluate accurate reflection intensities, especially for the weakest reflections, and multiple averaging of diffraction patterns enabled us to achieve very low random error levels. The final average estimated errors in F_N were 1.5% at low resolution (26–7 Å) and 3.3% at higher resolution (7–5 Å) and those in F_D were 1.2 and 4.8%, respectively. Relative to average F_N the expected signal for the total of 2.01 Pb^{2+} cited is 2.5% at low resolution and 5.9% at higher resolution. Since the extracted amplitudes for each reflection was evaluated from multiple observations (usually 24 for Na^+ PM and 36 for Pb^{2+} PM patterns) the random errors tend to cancel while the signal is reinforced. Based on the estimated error levels in F's we find, as shown in Figs. 5, *a* and *b*, that a signal from 0.24 Pb^{2+} (~3 electrons) can be distinguished from random noise. We had collected data to ~4 Å for some of the patterns, and a difference map synthesized at 4.5 Å (map not shown) showed essentially the same set of peaks as the 5 Å map (Fig. 1 *a*). However, this higher resolution map was noisier since the noise level in the difference map increases at least as $\sqrt{(\Sigma[\Delta F]^2)}$, coupled with the fact that the systematic errors in the extracted F's due to possible residual errors in the calculated tilt parameters increases with resolution and the average noise levels in the extracted amplitudes were also found to increase with resolution.

Previously Katre et al. (1986) from this laboratory synthesized Pb^{2+} PM – Ca^{2+} PM difference maps from x-ray powder diffraction data and located partially occupied Pb^{2+} sites on bR, which were found to be on helices 2, 3, 6, and 7. Our sites (i), (iv), and (v) on helices 7, 3, and between helices 2 and 3, respectively, are close to three of the four sites found by Katre et al. (1986). We find one additional site (vi) on helix 2, and two new sites on helix 4 and helix 5.

Since a ratio of 3 Pb^{2+} to bR was used both in this study and in our earlier x-ray work, we discuss below possible sources for the differences in the number and locations of some of the divalent cation sites in the two investigations. (*a*) In comparison there were far fewer independent observations in the x-ray powder pattern (7 Å against 5 Å resolution data used here) which was further reduced by rotational overlap of $F(hk)$ on $F(kh)$ in the x-ray work that could result in errors in the refinement due to insufficient data/parameter ratio. (*b*) Reconstituted PM generated by titrating blue membrane with 150-fold amounts of Na^+, as in this study, is essentially identical to native PM in its absorption and photocycle properties (Kimura et al., 1984; Chang et al., 1986), indicating a native-like protein conformation. Even though spectroscopically, Ca^{2+} reconstituted (used in x-ray work) and Na^+ reconstituted PM (in this study) appear very similar, possible small localized conformational differences at the cation binding pockets and/or different site-specific bind-

ing affinities for Na^+ could elicit slightly different "native" structures. This would effect the difference maps and the occupancies at the Pb^{2+} sites in the two maps. (*c*) Different sample preparation techniques resulting in possible differences in protein conformation in the hydrated membrane stack used in x-ray work and glucose-embedded sheets used in this study.

The binding characteristics of cations, particularly divalent cations, in the process of blue to purple transition have been recently investigated by optical absorption (Kimura et al., 1984; Zubov et al., 1986; Chang et al., 1986; Ariki and Lanyi, 1986) or by ESR (Duñach et al., 1986, 1987; Corcoran et al., 1987). Duñach et al. (1987), find five medium and high affinity sites (with K_d = 0.6–26.0 μM at pH 5.0 and 20–50 μM at pH 7.0) and five low-affinity sites (50 mM) for Mn^{2+} on bR. On the other hand, monovalent cations such as Na^+ or K^+ bind PM only weakly with affinity constants in the millimolar range and effect the blue to purple transition in millimolar concentrations as compared with micromolar concentration in the case of divalent cations. Trivalent cations such as La^{3+}, at pH 7.0, and at micromolar concentrations induce the blue to purple transition but affect the proton uptake by significantly reducing the decay of the M-intermediate and also reduce the amplitude of the O-intermediate (Chang et al., 1986). It is not yet clear whether the blue to purple transition effected by cations is due to a neutralization of the negative surface potential, (e.g., on the cytoplasmic surface, where apart from the excess negatively charged residues phospholipids are also assumed to be asymmetrically disposed [Henderson et al., 1978]), or in addition conformational effects induced by cation binding are also involved. Szundi and Stoeckenius (1987, 1988) argue from studies on lipid-depleted and lipid-substituted (acidic native lipids by neutral or zwitterionic lipids) membranes that the maintenance of purple color does not require cations. This was based on their observation that upon deionization the lipid-exchanged or lipid-depleted membranes did not change to blue. However, by pH reduction to ~1.0 they could generate blue-like membranes (λ_{max} = 585 nm compared with 605 nm for native blue membranes). In so far as the lipid-depleted or lipid-substituted membranes could be thought of as adequate models for the native PM, the results of Szundi and Stoeckenius do not preclude the existence of specific protein binding sites for divalent cations or, as stated by these authors, the extent to which cations affect the surface charge may also effect the purple to blue transition. On the other hand, Chang et al. (1986) from atomic absorption spectroscopy and Duñach et al. (1986) from ESR observe that bleached deionized membranes bind fewer divalent cations and more weakly than do deionized membranes. Because PM does not change its surface potential upon bleaching (Ehrenberg and Meiri, 1983; Packer et al., 1984), these observations probably indicate that specific conformational interactions between surface residues and divalent cations are also present. Indeed, circular dichroism (Kimura et al., 1984) and thermal denaturation (Chang et al., 1986) data suggest that chelation by divalent cation induces protein conformational changes. Also, Duñach et al. (1988) have observed that addition of Mn^{2+} to a deionized purple membrane at pH 6.5 induces a UV-difference spectrum, indicating that a conformational change is occurring. However, these authors also find similar difference upon pH increase of the blue membrane suspensions and have raised the question about the possible functional role of the cation-induced conformational change.

In this work we have carefully examined whether there are discrete binding sites for divalent cation on single PM sheets under the nominal functionally active 3:1 Pb^{2+} to bR reconstitution. After careful consideration of all sources of error, our finding that none of the sites located in projection are fully occupied could lead to two alternate suggestions. These are either that these sites represent binding pockets that are indeed preferential rather than specific or that the drying from solution on the electron microscopy grid in a glucose environment statistically disorders the probably flexible bR surface residues (Jaffe and Glaeser, 1987), where the cations are most expected to bind, to reduce the effective occupancies. If the latter is the case then the relatively higher occupancy sites at helices 4 and 5 could represent discrete sites where binding of divalent cation could exert electrostatic and/or allosteric effects, for instance, in stabilizing the M_{412} intermediate in the native purple membrane. In this context, of particular interest are the putative linking regions between the helices on the cytoplasmic surface that contain 4 Asp (36, 38, 102, 104) and 2 Glu (161, 166) residues (see Katre and Stroud, 1981). Selective alterations in side-chain length and charge of these carboxylic acid residues by site-specific mutation will test their involvement in cation binding as well as their possible influence on the blue to purple transition.

An important feature of this present study is that we have demonstrated that we can distinguish in our difference map a signal from about one quarter of Pb^{2+} ion from random noise. This translates to a change of ~1.5 carbon atoms corresponding, for example, to an isomorphous replacement of an Ala to Thr. Thus, the methods described here provide a powerful high resolution assay for structure change that is sensitive at the level of less than two carbon atoms difference. The scheme we describe to extract accurate values of intensities from low-dose electron diffraction patterns by using a matched-filter algorithm, and for correcting these extracted intensities for twinning and specimen tilt, is capable of assessing whether the structural consequences

of any given site-directed mutagenic change are localized just to the residue that is the site of substitution or involve large scale movements. In conjunction with spectroscopic studies, a high resolution assay for structural change makes it possible to determine whether an effect on bR function is direct or is a consequence of alteration relayed to the rest of the protein.

APPENDIX

For a P3 lattice in general, three types of twinning operations are possible that combine the structure factor $F(hkl)$ with those for three other twin-related reflections. The three possible twin components are (a) reflections of the type $(\overline{h+k}, k, l)$ due to patches related by twofolds parallel to (100), (010), or ($\bar{1}10$); (b) reflections of the type (khl) due to patches related by twofolds parallel to (110), ($\bar{1}20$), or ($2\bar{1}0$), and (c) reflections of the type $(\bar{h}\bar{k}l)$, due to patches related by twofold axis perpendicular to the membrane: these are Friedel related to (hkl) only for untilted two-dimensional crystalline patch ($F(\bar{h}\bar{k}l) = F(hkl)$ for $l = 0$). Denoting by X_1, X_2, X_3, and X_4, the fractional volumes of the four twin-related patches and by G the twinned-tilted intensity of the hkz^*_{hk} reflection we have

$$G = X_1 I(hkz^*_{hk}) + X_2 I(\bar{h}+k, k, z^*_{hk}) + X_3 I(khz^*_{hk}) + X_4 I(\bar{h}\bar{k}z^*_{hk}), \quad (1)$$

where

$$X_1 + X_2 + X_3 + X_4 = 1.0 \text{ with } X_i \geq 0.0. \quad (2)$$

In Eq. 1, I is the untwinned intensity and z^*_{hk} is the reciprocal lattice coordinate normal to the two-dimensional lattice given as

$$z^*_{hk} = a^* \tan\theta[h \sin\psi + k \sin(\psi + 60°)]. \quad (3)$$

In Eq. 3, θ is the tilt angle and ψ is the angle between the tilt axis and the a^* axis. For small amounts of tilt we can express

$$I(hkz^*_{hk}) = I°(hk) + q_1(hk)z^*_{hk} + \ldots \text{ higher order terms}, \quad (4)$$

where $I°(hk)$ is the untilted-untwinned intensity and $q_j(hk)$ are the various orders of derivatives of the intensity profile at $z^*_{hk} = 0.0$. Using Eq. 4 for the various terms in Eq. 1 we get

$$G = (X_1 + X_4)I°(hk) + (X_3 + X_2)I°(kh) + T(hk), \quad (5)$$

where the tilt containing term $T(hk)$ is given by

$$T(hk) = z^*_{hk}(q_1(hk)(X_1 - X_4) + q_1(kh)(X_3 - X_2) + \text{higher-order terms}. \quad (6)$$

The three independent twin parameters, the two tilt parameters (θ and ψ), and K and B, the scale and temperature factors, are obtained by least-squares minimizing the sum H calculated over all reflections to 7 Å where H is given by,

$$H = \sum_{hk} (1/\sigma_{hk})^2 [G - [(X_1 + X_4)I°(hk) + (X_3 + X_2)I°(kh) + T(hk)] \cdot K \exp(-B s^2)]^2. \quad (7)$$

In Eq. 7 σ_{hk} is the observed standard deviation for the sixfold symmetry mates of the twinned-tilted reflection hk, s is the reciprocal lattice vector, and we approximate the intensities at zero tilt $I°$ by the values obtained by Hayward and Stroud (1981) from native unreconstituted (untwinned) nominally untilted patches. Also in Eq. 7 the values used for the derivatives $q_j(hk)$ were calculated from the three-dimensional tilt data for the set of up to 7-Å resolution reflections as used in Katre et al., 1986. From Eq. 4 we can form the simultaneous equations:

$$(X_1 + X_4)I°(hk) + (X_3 + X_2)I°(kh) + T(hk) = G'(h, k, z^*_{hk}) \quad (8a)$$

$$(X_1 + X_4)I°(kh) + (X_3 + X_2)I°(hk) + T(kh) = G'(k, h, z^*_{kh}), \quad (8b)$$

where $G' = G/K \exp(-Bs^2)$.

These yield detwinned-detilted intensities $I(hk)$ and also $I(kh)$. For reflections of resolution greater than 7 Å (5–7 Å), using the knowledge of the already determined tilt parameters to evaluate z^* for these reflections and using a linear approximation for the tilt term in Eq. 5, the detwinned-detilted intensity values were extracted after a linear fit to the intensities of the sixfold symmetry related mates.

We thank Nandini Katre and Janet Finer-Moore for useful discussions. A. K. Mitra thanks Thomas Earnest for useful comments. We are grateful to Professor Walther Stoeckenius for generously providing purple membranes.

Research was supported by the National Institutes of Health grant GM32079 to Robert M. Stroud.

Received for publication 24 June 1988 and in final form 17 October 1989

Note added in proof: Stoeckenius, W., and I. Szundi in a recent publication (1989. *Biophys. J.* 56:369–383) provide theoretical justification to their earlier work (referred to in text) on the purple to blue transition in PM with surface charge modified by lipid depletion or lipid substitution. However, as before, their results cannot dispute specific or preferential binding of divalent cation to native PM nor to the possible role of such binding.

REFERENCES

Ariki, M., and J. K. Lanyi. 1986. Characterization of metal ion-binding sites in bacteriorhodopsin. *J. Biol. Chem.*261:8167–8174.

Baldwin, J. M., R. Henderson, E. Beckman, and F. Zemlin. 1988. Images of purple membrane at 2.8 Å resolution obtained by cryo-electron microscopy. *J. Mol. Biol.* 202:585–591.

Bayley, H., K.-S. Huang, R. Ramakrishnan, A. H. Ross, Y. Tagagaki, and H. G. Khorana. 1981. Site of attachment of retinal in bacteriorhodopsin. *Proc. Natl. Acad. Sci. USA.* 78:2225–2229.

Bevington, P. R. 1969. Data Reduction and Error Analysis for the Physical Sciences. McGraw-Hill Book Company, New York. 73 pp.

Bogomolni, R. A., R. A. Baker, R. H. Lozier, and W. Stoeckenius. 1976. Light-driven proton translocations in halobacterium halobium. *Biochim. Biophys. Acta.* 440:68–88.

Blundell, T. L., and L. N. Johnson. 1976. Protein Crystallography. Academic Press Inc., London. 409–411.

Chang, C.-H., J.-G. Chen, R. Govindjee, and T. Ebrey. 1985. Cation binding by bacteriorhodopsin. *Proc. Natl. Acad. Sci. USA.* 82:396–400.

Chang, C.-H., R. Jonas, S. Melchiore, R. Govindjee, and T. G. Ebrey. 1986. Mechanism and role of divalent cation binding of bacteriorhodopsin. *Biophys. J.* 49:731–739.

Cherry, R. J., U. Muller, R. Henderson, and M. P. Heyn. 1978. Temperature-dependent aggregation of bacteriorhodopsin in dipalmitoyl- and dimyristoylphosphatidylcholine vesicles. *J. Mol. Biol.* 121:283–298.

Chronister, E. L., and M. A. El-Sayed. 1987. Time-resolved resonance Raman spectra of the photocycle intermediates of acid and deionized bacteriorhodopsin. *Photochem. Photobiol.* 45:507–513.

Corcoran, T. C., K. Z. Ismail, and M. A. El-Sayed. 1987. Evidence for the involvement of more than one metal cation in the Schiff base deprotonation process during the photocycle of bacteriorhodopsin. *Proc. Natl. Acad. Sci. USA.* 84:4094–4098.

Dickerson, R. E., J. E. Weinzierl, and R. A. Palmer. 1968. A least squares refinement method for isomorphous replacement. *Acta Crystallogr. Sect. B. Struct. Crystallogr. Cryst. Chem.* B24:997–1003.

Duñach, M., M. Seigneuret, J.-L. Rigaud, and E. Padros. 1986. The relationship between chromophore moiety and the cation binding sites in bacteriorhodopsin. *Biosci. Rep.* 6:961–966.

Duñach, M., M. Seigneuret, J.-L. Rigaud, and E. Padros. 1987. Characterization of the cation binding sites of the purple membrane. Electron spin resonance and flash photolysis studies. *Biochemistry.* 26:1179–1186.

Duñach, M., E. Padros, M. Seigneuret, and J.-L. Rigaud. 1988. On the molecular mechanism of the blue to purple transition of bacteriorhodopsin. UV-difference spectroscopy and electron spin resonance studies. *J. Biol. Chem.* 263:7555–7559.

Dupuis, P., T. C. Corcoran, and M. A. El-Sayed. 1985. Importance of bound divalent cations to the tyrosine deprotonation during the photocycle of bacteriorhodopsin. *Proc. Natl. Acad. Sci. USA.* 82:3662–3664.

Ehrenberg, E., and Z. Meiri. 1983. The bleaching of purple membranes does not change their surface potential. *FEBS (Fed. Eur. Biochem. Soc.) Lett.* 164:63–66.

Engelman, D. M., R. Henderson, A. D. McLachlan, and B. A. Wallace. 1980. Path of polypeptide in bacteriorhodopsin. *Proc. Natl. Acad. Sci. USA.* 77:2023–2027.

Glaeser, R. M., J. S. Jubb, and R. Henderson. 1985. Structural comparison of native and deoxycholate-treated purple membrane. *Biophys. J.* 48:775–780.

Hayward, S. B., and R. M. Stroud. 1981. Projected structure of purple membrane determined to 3.7 Å resolution by low temperature electron microscopy. *J. Mol. Biol.* 151:491–517.

Henderson, R., J. S. Jubb, and S. Whytock. 1978. Specific labelling of the protein and lipid on the extracellular surface of the purple membrane. *J. Mol. Biol.* 123:259–274.

Hoel, P. G. 1984. Introduction to Mathematical statistics. Fifth ed. John Wiley and Sons, New York. 193 pp.

Jaffe, J. S., and R. M. Glaeser. 1987. Difference Fourier analysis of "surface features" of bacteriorhodopsin using glucose-embedded and frozen-hydrated purple membrane. *Ultramicroscopy.* 23:17–28.

Katre, N. V., and R. M. Stroud. 1981. A probable linking sequence between two transmembrane components of bacteriorhodopsin. *FEBS (Fed. Eur. Biochem. Soc.) Lett.* 136:170–174.

Katre, N. V., P. K. Wolber, W. Stoeckenius, and R. M. Stroud. 1981. Attachment site of retinal in bacteriorhodopsin. *Proc. Natl. Acad. Sci. USA.* 78:4068–4072.

Katre, N. V., S. Hayward, and R. M. Stroud. 1984. Location of an extrinsic label in the primary and tertiary structure of bacteriorhodopsin. *Biophys. J.* 46:195–203.

Katre, N. V., Y. Kimura, and R. M. Stroud. 1986. Cation binding sites on the projected structure of bacteriorhodopsin. *Biophys. J.* 50:277–284.

Kimura, Y., A. Ikegami, and W. Stoeckenius. 1984. Salt and pH-dependent changes of the purple membrane absorption spectrum. *Photochem. Photobiol.* 40:641–646.

Kobayashi, T., H. Ohtani, J.-I. Iwai, A. Ikegani, and H. Uchiki. 1983. Effect of pH on the photoreaction cycle of bacteriorhodopsin. *FEBS (Fed. Eur. Biochem. Soc.) Lett.* 162:197–200.

Mowery, P. C., R. H. Lozier, Q. Chae, Y.-W. Tseng, M. Taylor, and W. Stoeckenius. 1979. Effect of acid pH on the absorption spectra and photoreactions of bacteriorhodopsin. *Biochemistry.* 18:4100–4107.

Oesterhelt, D., and W. Stoeckenius. 1974. Isolation of the cell membrane of Halobacterium and its fractionation into red and purple membrane. *Methods Enzymol.* 31:667–678.

Packer, L., B. Arrio, G. Johannin, and P. Volfin. 1984. Surface charge of purple membrane measured by laser Doppler velocimetry. *Biochem. Biophys. Res. Commun.* 122:252–258.

Spencer, S. A., and A. A. Kossiakoff. 1980. An automated peak fitting procedure for processing protein diffraction data from a linear position-sensitive detector. *J. Appl. Crystallogr.* 13:563–571.

Szundi, I., and W. Stoeckenius. 1987. Effect of lipid surface charges on the purple-to-blue transition of bacteriorhodopsin. *Proc. Natl. Acad. Sci. USA.* 84:3681–3684.

Szundi, I., and W. Stoeckenius. 1988. Purple-to-blue transition of bacteriorhodopsin in a neutral lipid environment. *Biophys. J.* 54:227–232.

Stoeckenius, W., R. H. Lozier, and R. A. Bogomolni. 1979. Bacteriorhodopsin and the purple membrane of halobacteria. *Biochim. Biophys. Acta.* 505:215–278.

Tsygannik, I. N., and J. M. Baldwin. 1987. Three-dimensional structure of deoxycholate-treated purple membrane at 6 Å resolution and molecular averaging of three crystal forms of bacteriorhodopsin. *Eur. Biophys. J.* 14:263–272.

Zubov, B., K. Tsuji, and B. Hess. 1986. Transition kinetics of the conversion of blue to purple bacteriorhodopsin upon magnesium binding. *FEBS (Fed. Eur. Biochem. Soc.) Lett.* 200:226–230.